Simultaneous Train Localization and Radio Transmitter Mapping with TDoA and Magnetic Field Measurements

Benjamin Siebler*, Stephan Sand*, and Uwe D. Hanebeck†
*German Aerospace Center (DLR), Institute of Communications and Navigation
†Karlsruhe Institute of Technology (KIT), Intelligent Sensor-Actuator-Systems Laboratory (ISAS)
benjamin.siebler@dlr.de

***Abstract*—This paper proposes a simultaneous localization and mapping (SLAM) algorithm that jointly estimates the position of a train on a railway track and the positions of track-side radio transmitters to enable accurate train localization in areas where satellite-based systems are not available. The algorithm uses odometer and magnetometer measurements and combines them with signal of opportunity time difference of arrival (TDoA) measurements to track-side radio transmitters. To solve the SLAM problem, pose-graph optimization is combined with a magnetic field-based loop closure detection that exploits the position dependent distortions in the Earth magnetic field encountered along railway tracks. We demonstrate the feasibility of the algorithm in an evaluation with real odometer and magnetometer measurements from the railway domain and simulated TDoA measurements. The evaluation shows that the SLAM algorithm enables long-term stable train position estimation and that the radio transmitters can be localized with meter-level accuracy.**

I. Introduction

Railway localization is considered as one of the key technologies for automating railway traffic. Most research in this area is focused on the use of global navigation satellite systems (GNSS) and how its integrity can be ensured. GNSS is an important part of future train localization systems, but needs to be combined with other sensor modalities. This need is a result of the vulnerability of GNSS receivers to jamming and spoofing and the fact that the GNSS receiver antenna needs a line of sight to the satellites. If the line of sight is blocked, e.g., due to shadowing in urban areas or tunnels, a reliable position solution cannot be obtained.

In our work, we therefore focus on the development of a magnetic field-based localization system for railways and showed its feasibility, e.g., in [1]. The idea of magnetic localization is based on the observation that the Earth's magnetic field is strongly distorted by magnetic material alongside the tracks. A common example for such magnetic material is steel found in the rails, signal poles, and reinforced concrete. When the magnetic material is located at fixed positions relative to the track also the distortions it causes are fixed. Each part of a track therefore has a characteristic magnetic "fingerprint" that can be used for absolute positioning. The use of the magnetic field for localization is not only feasible in the railway domain but also has been proposed for the air space [2], roads [3], and indoor environments [4], [5], [6].

The simplest way to utilize the magnetic field for localization is to create a map of the magnetic field based on a reference localization system and then use this map to match a measurement sequence of a train-mounted magnetometer to it. Unfortunately, creating the magnetic maps is often problematic in practice since it requires a reference system that might not exist in all relevant environments such as tunnels. This results in a chicken-and-egg problem, for position estimation we need the magnetic field map and for mapping we need the position. This kind of problem is well known under the name simultaneous localization and mapping (SLAM) and has been addressed specifically for magnetic localization, e.g., in [7] and [8]. While [7] and [8] use particle filters to solve the SLAM problem, in [9] we showed how pose-graph optimization and magnetic field-based loop closures can be used to address the SLAM problem in the railway domain. Our graph-based algorithm only requires an odometer and a low-cost magnetometer and has been shown to enable long-term stable train localization.

In this paper we now take our algorithm from [9] and extend it with the possibility to process time difference of arrival (TDoA) measurements to further improve the localization accuracy and to have a redundant source of absolute position information in the case the magnetic field cannot provide sufficient information or the magnetometer measurements are disturbed. Here we assume that we use signals of opportunity (SoO) for the TDoA measurements, e.g., from the future railway mobile communication system (FRMCS). Since we use SoO we cannot assume to know the track-side transmitter positions or that they are synchronized to each other. To measure a TDoA we thus follow our approach from [10] and use two train-mounted antennas connected to synchronized receivers. For the TDoA measurements the pose-graph optimization is extended to also estimate the unknown transmitter positions. In order to show the feasibility of the proposed algorithm, an evaluation is carried out with real magnetometer and odometer measurements from the railway domain and TDoA measurements simulated based on the parameters of FRMCS.

II. Methodology

A. SLAM as Maximum-A-Posteriori Estimation Problem

The proposed SLAM method is an extension of our pose-graph SLAM algorithm from [9]. The goal of the proposed algorithm is to estimate the train trajectory and the positions of the radio transmitters along the railway track by only

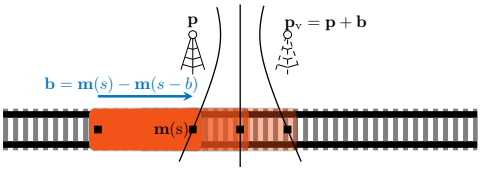

Figure 1. Three examples for the TDoA hyperbola for two antennas mounted on the roof of a train with a baseline b. If the transmitter position is assumed to be known, the hyperbolas represent all possible positions of the leading train antenna at position $\mathbf{m}(s)$. The hyperbolas are equivalent to the ones resulting from a single train antenna and two track-side transmitters. The second, virtual, transmitter is shifted relative to the physical transmitter by the 3D baseline vector $\mathbf{b}$.

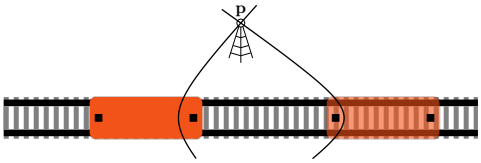

Figure 2. Two examples for the TDoA hyperbola when we assume known positions for the train antennas. The shown hyperbolas represent all points at which the transmitter can be located.

using magnetic field, odometer, and TDoA measurements. The TDoAs are measured relative to transmitters with unknown positions and as such the measurements only contain relative information w.r.t. the train and transmitter positions. For the remainder of the paper we will summarize all states that we want to estimate in the state vector $\mathbf{x}$

$$\mathbf{x} = \begin{bmatrix} s_1 & \cdots & s_K & \mathbf{p}_1 & \cdots & \mathbf{p}_N \end{bmatrix}^\top \ , \tag{1}$$

where the train trajectory is given by the K one-dimensional along-track positions $s_i \in [0, L]$ of the train on a track with length L and $\mathbf{p}_j \in \mathbb{R}^3$ is the unknown position of the j-th transmitter.

Formally, the SLAM algorithm tries to find the maximum-a-posteriori (MAP) estimate $\hat{\mathbf{x}}$ of state vector $\mathbf{x}$

$$\hat{\mathbf{x}} = \arg\max_{\mathbf{x}} \ \mathrm{p}(\mathbf{x} | \mathcal{Z}_{\text{mag}}, \mathcal{Z}_{\text{odo}}, \mathcal{Z}_{\tau}) \ , \tag{2}$$

where $\mathcal{Z}_{\text{mag}}$, $\mathcal{Z}_{\text{odo}}$ and $\mathcal{Z}_{\tau}$ are sets that contain the magnetic field, odometer, and TDoA measurements. The sets only contain relative position information. The odometer measurements contain information about the along-track distance of two consecutive train positions and the TDoA measurements solely depend on the Euclidean distance between the train and the transmitter antennas. This fits perfectly well to the idea of pose-graph SLAM that represents relative position information as edges between nodes that represent the state variables [11]. In contrast to $\mathcal{Z}_{\text{odo}}$ and $\mathcal{Z}_{\tau}$, $\mathcal{Z}_{\text{mag}}$ is not the set of magnetometer measurements, since these measurements do not directly contain relative position information, but a set of relative position information derived from the magnetometer measurements. In the following sections, this is further elaborated and detailed models for the different types of measurements are derived.

B. Measurement Models

1) TDoA Model: For the TDoA measurements we assume, similar to our prior work [10], that the train is equipped with two antennas connected to synchronized receivers. The mounting positions of the antennas on the train roof are shifted in along-track direction by a fixed baseline $b \in \mathbb{R}_{\geq 0}$. The TDoA then represents the time difference of arrival between these antennas relative to a single transmitter. For SLAM it is convenient to multiply the TDoA by the speed of light which yields the distance difference

$$\tau_i = \|\mathbf{m}(s_j) - \mathbf{p}_l\| - \|\mathbf{m}(s_j - b) - \mathbf{p}_l\| \ , \tag{3}$$

where $\mathbf{p}_l \in \mathbb{R}^3$ is the position of transmitter l and $\mathbf{m}(\cdot)$ is the geometrical map of the track that relates the along-track position s_j to its position in $\mathbb{R}^3$. The mapping between the i-th TDoA τ_i to the corresponding transmitter and along-track position is done by the index maps $j = \mathrm{I}_{\tau,s}(i)$ and $l = \mathrm{I}_{\tau,\mathbf{p}}(i)$.

By using two antennas on the train we do not require the existence of two synchronized transmitters to measure a TDoA, which enables us to use a broad spectrum of SoO, e.g., from cellular systems. In Fig. 1 and Fig. 2, the resulting TDoA hyperbolas are shown. Figure 1 shows the scenario where the transmitter position is known and we want to localize the leading train antenna at position $\mathbf{m}(s)$. In this scenario, from a geometrical point of view, measuring the TDoA with two receiver antennas is equivalent to the case of having two synchronized transmitters which are shifted relative to each other. The position of the second, virtual, transmitter is shifted relative to the physical one by the baseline vector $\mathbf{b} = \mathbf{m}(s) - \mathbf{m}(s-b)$. Note, for a curved track it is assumed that the baseline b between the antennas is small w.r.t. the track curvature and therefore the length of the track between the antennas is $\approx b$. This approximation is quite accurate for baselines $\leq 20\,\mathrm{m}$, which we use in the following. Figure 2 shows the hyperbola for the scenario where the train antenna position is known and the transmitter position is unknown. In this scenario, the hyperbolas for different train positions intersect at the transmitter position, which enables the SLAM algorithm to estimate the transmitter position.

For the TDoA measurement, additive white Gaussian noise (AWGN) is considered yielding the measurement model

$$z_{i,\tau} = \tau_i + n_{i,\tau} \ , \tag{4}$$

with Gaussian noise $n_{i,\tau} \sim \mathcal{N}(0, \sigma^2_{i,\tau})$. For the SLAM algorithm introduced in the next section, we will need an explicit expression of the log-likelihood of each measurement. For TDoA, the log-likelihood is directly obtained from (3), (4),

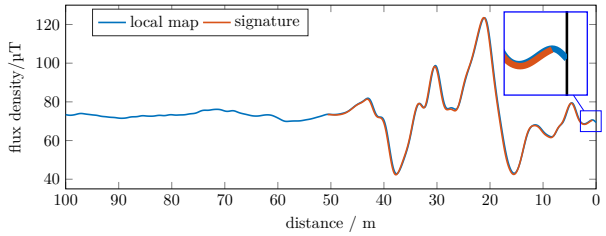

Figure 3. Loop closure found from the correlation of a 50 m long magnetic signature (red) with a 100 m long local map (blue). The signature is shifted relative to the local map (magnified part) such that the correlation coefficient is maximized. The shift maximizing the correlation coefficient will be used as observation $z_{i,\text{mag}}$ for $\Delta s_{i,\text{mag}}$.

and the measurement noise as

$$\begin{aligned}\ln \mathrm{p}(z_{i,\tau}|\mathbf{x}) &= \ln \mathcal{N}\left(z_{i,\tau}; \tau_i, \sigma_{i,\tau}^2\right) \\ &= \ln \frac{1}{\sigma_{i,\tau}\sqrt{2\pi}} - \frac{(z_{i,\tau}-\tau_i)^2}{2\sigma_{i,\tau}^2} \\ &= \ln \frac{1}{\sigma_{i,\tau}\sqrt{2\pi}} - \frac{\mathrm{e}_{i,\tau}(\mathbf{x})^2}{2\sigma_{i,\tau}^2} = \lambda_{i,\tau}(\mathbf{x}) \ . \end{aligned} \tag{5}$$

In the last line we introduced the error function $\mathrm{e}_{i,\tau}(\mathbf{x})$ of the i-th TDoA measurement, which in essence is the difference between the actual measurement $z_{i,\tau}$ and its mean τ_i.

2) Magnetometer Model: As mentioned before, the set $\mathcal{Z}_{\text{mag}}$ is not directly the set of magnetometer measurements, but rather a set of relative position information derived from the magnetometer measurements. Each element $z_{i,\text{mag}} \in \mathcal{Z}_{\text{mag}}$ represents the along-track distance between two along-track positions

$$\Delta s_{i,\text{mag}} = s_{\mathrm{I}_{\text{mag,first}}(i)} - s_{\mathrm{I}_{\text{mag,second}}(i)} \ , \tag{6}$$

where $\mathrm{I}_{\text{mag,first}}(i)$ and $\mathrm{I}_{\text{mag,second}}(i)$ are simple index maps that associate $\Delta s_{i,\text{mag}}$ with the corresponding positions.

To obtain observations of $\Delta s_{i,\text{mag}}$, we perform a magnetic field-based loop closure detection. Here we give only a brief description of the general idea, more details on this can be found in [9]. The magnetic field-based loop closure detection exploits that the magnetic field at the same along-track position stays constant over time. For the loop closure detection the SLAM algorithm stores for each along-track position in $\mathbf{x}$ a local map of the magnetic field that represents the magnetic field of a short piece of track that was traversed by the train before reaching the corresponding along-track position. The local map is created from the measured magnetometer time series by transforming it in the spatial domain using the odometer data that measures how far the train travels between the different magnetometer measurements. With the local maps we can now detect a loop closure by checking if two local maps show a high similarity. More concretely, for each position s_i in $\mathbf{x}$ the corresponding local map is compared to the local maps of all other positions s_j with $j \neq i$ that are within a certain search interval. In the comparison the local map of s_i is truncated to obtain a "magnetic signature" that can be shifted over the other local maps. For each possible shift within a local map then the correlation coefficient is calculated. The resulting correlation coefficients are compared to a threshold and when the threshold is exceeded a loop closure is detected. For each loop closure we then add an observation $z_{i,\text{mag}}$ to $\mathcal{Z}_{\text{mag}}$, where $z_{i,\text{mag}}$ is the shift in the local map at which the highest correlation coefficient was observed. An example of a successful match of a magnetic signature to a local map is shown in Fig. 3.

Since the correlation coefficient between the local map and the magnetic signature is affected by measurement noise and an imperfect spatial transformation, we assume that $z_{i,\text{mag}}$ is a noisy observation of the true along-track distances $\Delta s_{i,\text{mag}}$ with log-likelihood

$$\begin{aligned}\ln \mathrm{p}(z_{i,\text{mag}}|\mathbf{x}) &= \ln \frac{1}{\sigma_{i,\text{mag}}\sqrt{2\pi}} - \frac{(z_{i,\text{mag}}-\Delta s_{i,\text{mag}})^2}{2\sigma_{i,\text{mag}}^2} \\ &= \ln \frac{1}{\sigma_{i,\text{mag}}\sqrt{2\pi}} - \frac{\mathrm{e}_{i,\text{mag}}(\mathbf{x})^2}{2\sigma_{i,\text{mag}}^2} = \lambda_{i,\text{mag}}(\mathbf{x}) \ . \end{aligned} \tag{7}$$

3) Odometer Model: The odometer simply measures the traveled distance over time. Therefore, the odometer measurements are a direct observation of the along-track distance between two consecutive along-track positions in $\mathbf{x}$

$$\Delta s_{i,\text{odo}} = s_{\mathrm{I}_{\text{odo}}(i)} - s_{\mathrm{I}_{\text{odo}}(i)-1} \ , \tag{8}$$

where $\mathrm{I}_{\text{odo}}(i)$ is a function that relates the i-th odometer measurement to the corresponding along-track position in $\mathbf{x}$. Since the odometer always measures the distance the train has traveled between two consecutive positions, e.g., the distance between s_1 and s_2, we can use $\mathrm{I}_{\text{odo}}(i) - 1$ for the index of the second position in (8). As for the other measurements, the odometer is assumed to be affected by AWGN, which results in the log-likelihood

$$\begin{aligned}\ln \mathrm{p}(z_{i,\text{odo}}|\mathbf{x}) &= \ln \frac{1}{\sigma_{i,\text{odo}}\sqrt{2\pi}} - \frac{(z_{i,\text{odo}}-\Delta s_{i,\text{odo}})^2}{2\sigma_{i,\text{odo}}^2} \\ &= \ln \frac{1}{\sigma_{i,\text{odo}}\sqrt{2\pi}} - \frac{\mathrm{e}_{i,\text{odo}}(\mathbf{x})^2}{2\sigma_{i,\text{odo}}^2} = \lambda_{i,\text{odo}}(\mathbf{x}) \ . \end{aligned} \tag{9}$$

C. Factorization of the Posterior

In order to find the MAP estimate (2) it is beneficial to reformulate the posterior in terms of the likelihood and the state prior

$$\mathrm{p}(\mathbf{x}|\mathcal{Z}_{\text{mag}}, \mathcal{Z}_{\text{odo}}, \mathcal{Z}_{\tau}) \propto \mathrm{p}(\mathcal{Z}_{\text{mag}}, \mathcal{Z}_{\text{odo}}, \mathcal{Z}_{\tau}|\mathbf{x})\, \mathrm{p}(\mathbf{x}) \ . \tag{10}$$

Assuming the different types of observation are conditionally independent, the likelihood can be factored into three parts

$$\mathrm{p}(\mathcal{Z}_{\text{mag}}, \mathcal{Z}_{\text{odo}}, \mathcal{Z}_{\tau}|\mathbf{x}) = \mathrm{p}(\mathcal{Z}_{\text{mag}}|\mathbf{x})\, \mathrm{p}(\mathcal{Z}_{\text{odo}}|\mathbf{x})\, \mathrm{p}(\mathcal{Z}_{\tau}|\mathbf{x}) \ . \tag{11}$$

For the maximization we now take (11) and plug it into the right hand side of (10) and take the logarithm. Taking the logarithm transforms the products into sums and the maximization from (2) becomes

$$\hat{\mathbf{x}} = \arg\max_{\mathbf{x}} \ln \mathrm{p}(\mathcal{Z}_{\text{mag}}, \mathcal{Z}_{\text{odo}}, \mathcal{Z}_{\tau}|\mathbf{x}) + \ln \mathrm{p}(\mathbf{x}) \ , \tag{12}$$

where the first term is given by

$$\ln \mathrm{p}(\mathcal{Z}_{\text{mag}}, \mathcal{Z}_{\text{odo}}, \mathcal{Z}_{\tau} | \mathbf{x}) = \underbrace{\ln \mathrm{p}(\mathcal{Z}_{\text{mag}}|\mathbf{x})}_{\lambda_{\text{mag}}(\mathbf{x})} + \underbrace{\ln \mathrm{p}(\mathcal{Z}_{\text{odo}}|\mathbf{x})}_{\lambda_{\text{odo}}(\mathbf{x})} + \underbrace{\ln \mathrm{p}(\mathcal{Z}_{\tau}|\mathbf{x})}_{\lambda_{\tau}(\mathbf{x})} \ . \quad (13)$$

The cost function in (12) contains now one term for each kind of measurement and one term for the prior information. For all types of observation we assume that two observations of the same type are mutual independent given $\mathbf{x}$. Under that assumption we can easily find the concrete equations for the joint log-likelihoods by using (5), (7), (9)

$$\lambda_{\text{mag}}(\mathbf{x}) = \sum_{i=1}^{|\mathcal{Z}_{\text{mag}}|} \lambda_{i,\text{mag}}(\mathbf{x}) \quad \lambda_{\text{odo}}(\mathbf{x}) = \sum_{i=1}^{|\mathcal{Z}_{\text{odo}}|} \lambda_{i,\text{odo}}(\mathbf{x})$$
$$\lambda_{\tau}(\mathbf{x}) = \sum_{i=1}^{|\mathcal{Z}_{\tau}|} \lambda_{i,\tau}(\mathbf{x}) \ . \quad (14)$$

For the posterior term in (12) a simple Gaussian prior is considered, in which the different states are independent

$$\ln \mathrm{p}(\mathbf{x}) = \sum_{i=1}^{K} \ln \mathcal{N}(s_i; \mu_{i,s}, \sigma_{i,s}^2) + \sum_{i=1}^{N} \ln \mathcal{N}(\mathbf{p}_i; \boldsymbol{\mu}_{i,\mathbf{p}}, \boldsymbol{\Sigma}_{i,\mathbf{p}}) \ . \quad (15)$$

Note, the along-track position is scalar and the transmitter positions are vectors. Therefore, the priors for the along-track positions are univariate Gaussians with mean $\mu_{i,s}$ and standard deviation $\sigma_{i,s}$ and the priors for the transmitter positions are multivariate Gaussians with mean vector $\boldsymbol{\mu}_{i,\mathbf{p}}$ and covariance matrix $\boldsymbol{\Sigma}_{i,\mathbf{p}}$.

With (12)–(15) we now have an explicit expression of the optimization cost function. For the actual optimization we can ignore all additive terms that are independent from the estimated state. Furthermore, we will transform the maximization problem into a minimization problem by multiplying the cost function with -2. The MAP estimation problem can now be formulated as

$$\hat{\mathbf{x}} = \arg\min_{\mathbf{x}} \mathrm{c}_{\text{lik}}(\mathbf{x}) + \mathrm{c}_{\text{prior}}(\mathbf{x}) \ , \quad (16)$$

with the cost function for the measurements

$$\mathrm{c}_{\text{lik}}(\mathbf{x}) = \sum_{i=1}^{|\mathcal{Z}_{\tau}|} \frac{\mathrm{e}_{i,\tau}(\mathbf{x})^2}{\sigma_{i,\tau}^2} + \sum_{i=1}^{|\mathcal{Z}_{\text{mag}}|} \frac{\mathrm{e}_{i,\text{mag}}(\mathbf{x})^2}{\sigma_{i,\text{mag}}^2} + \sum_{i=1}^{|\mathcal{Z}_{\text{odo}}|} \frac{\mathrm{e}_{i,\text{odo}}(\mathbf{x})^2}{\sigma_{i,\text{odo}}^2} \ , \quad (17)$$

and the cost function for the prior

$$\mathrm{c}_{\text{prior}}(\mathbf{x}) = \sum_{i=1}^{K} \frac{\mathrm{e}_{i,s}(\mathbf{x})^2}{\sigma_{i,s}^2} + \sum_{i=1}^{N} \mathbf{e}_{i,\mathbf{p}}(\mathbf{x})^{\top} \boldsymbol{\Sigma}_{i,\mathbf{p}}^{-1} \mathbf{e}_{i,\mathbf{p}}(\mathbf{x}) \ . \quad (18)$$

For the prior the error functions are given by the differences between the current values of the states and their means

$$\mathrm{e}_{i,s}(\mathbf{x}) = s_i - \mu_{i,s}$$
$$\mathbf{e}_{i,\mathbf{p}}(\mathbf{x}) = \mathbf{p}_i - \boldsymbol{\mu}_{i,\mathbf{p}} \ . \quad (19)$$

D. Optimization Algorithm

From (16)–(18) it becomes clear that the MAP estimate is the solution of a weighted least-squares (LS) problem. Depending on the error functions, the LS problem is either linear or nonlinear. In our case, the LS problem is nonlinear due to the nonlinearity of the error function $\mathrm{e}_{i,\tau}(\cdot)$ of the TDoA measurements. In $\mathrm{e}_{i,\tau}(\cdot)$, the nonlinearity is a result of the Euclidean norm between the train position and the transmitter position and the map $\mathbf{m}(\cdot)$ from the one-dimensional along-track position domain to $\mathbb{R}^3$.

As in [11], here the Levenberg–Marquardt algorithm will be used for optimization. For the optimization, we first linearize all error functions around a working point $\mathbf{x}_*$ by representing them by their first order Taylor series. For the magnetometer measurements, this results in

$$\tilde{\mathrm{e}}_{i,\text{mag}}(\mathbf{x}) = \mathrm{e}_{i,\text{mag}}(\mathbf{x}_*) + \mathbf{J}_{i,\text{mag}}(\mathbf{x} - \mathbf{x}_*) \ , \quad (20)$$

where $\mathbf{J}_{i,\text{mag}}$ is the Jacobian of the error function w.r.t. $\mathbf{x}$. In the same way the Taylor series of the other error functions can be derived by inserting the corresponding error function and their Jacobian, $\mathbf{J}_{i,\text{odo}}$, $\mathbf{J}_{i,\tau}$, $\mathbf{J}_{i,\mathbf{p}}$, or $\mathbf{J}_{i,s}$, into (20). For the magnetic field observations, the odometer measurements, and the priors, the Jacobians are constant and easily derived due to the linearity of their error functions. For $\mathrm{e}_{i,\text{mag}}$ and $\mathrm{e}_{i,\text{odo}}$ the Jacobian is just a zero row vector with a 1 and a -1 entry at the positions corresponding to the two along-track position in their means (6) and (8). For $\mathrm{e}_{i,s}$ the Jacobian is a zero row vector with a 1 at the i-th position. For $\mathbf{e}_{i,\mathbf{p}}$ the Jacobian is a $3 \times \dim(\mathbf{x})$ block matrix with an 3×3 identity matrix placed at the block that corresponds to $\mathbf{p}_i$ while the rest of the matrix is zero.

For the i-th TDoA measurements the Jacobian is more involved since it depends on one along-track position s_j and one transmitter position $\mathbf{p}_l$. Furthermore, the error function is nonlinear, which leads to a working point dependent Jacobian. The Jacobian of $\mathrm{e}_{i,\tau}$ is a row vector with zeros everywhere except the elements given by the gradient w.r.t. the along-track position s_j

$$[\mathbf{J}_{i,\tau}]_j = \frac{[\mathbf{m}(s_j - b) - \mathbf{p}_l]^{\top} \frac{\partial}{\partial s_j} \mathbf{m}(s_j - b)}{\|\mathbf{m}(s_j - b) - \mathbf{p}_l\|} - \frac{[\mathbf{m}(s_j) - \mathbf{p}_l]^{\top} \frac{\partial}{\partial s_j} \mathbf{m}(s_j)}{\|\mathbf{m}(s_j) - \mathbf{p}_l\|} \quad (21)$$

and the gradient w.r.t. the transmitter position $\mathbf{p}_l$

$$[\mathbf{J}_{i,\tau}]_{K+1+3(l-1):K+3l} = \frac{[\mathbf{m}(s_j) - \mathbf{p}_l]^{\top}}{\|\mathbf{m}(s_j) - \mathbf{p}_l\|} - \frac{[\mathbf{m}(s_j - b) - \mathbf{p}_l]^{\top}}{\|\mathbf{m}(s_j - b) - \mathbf{p}_l\|} \ , \quad (22)$$

where $[\mathbf{J}_{i,\tau}]_{m:n}$ stands for the part of the vector that contains the m-th up to the n-th element.

The linearized error functions are now plugged into the cost function (16) which yields

$$\tilde{\mathrm{c}}(\mathbf{x}) = \tilde{\mathrm{c}}_{\text{lik}}(\mathbf{x}) + \tilde{\mathrm{c}}_{\text{prior}}(\mathbf{x}) \ , \quad (23)$$

with the term $\tilde{\mathrm{c}}_{\text{lik}}(\mathbf{x})$ related to the likelihood

$$\tilde{\mathrm{c}}_{\text{lik}}(\mathbf{x}) = \sum_{i=1}^{|\mathcal{Z}_\tau|} \frac{\tilde{\mathrm{e}}_{i,\tau}(\mathbf{x})^2}{\sigma_{i,\tau}^2} + \sum_{i=1}^{|\mathcal{Z}_{\text{mag}}|} \frac{\tilde{\mathrm{e}}_{i,\text{mag}}(\mathbf{x})^2}{\sigma_{i,\text{mag}}^2} + \sum_{i=1}^{|\mathcal{Z}_{\text{odo}}|} \frac{\tilde{\mathrm{e}}_{i,\text{odo}}(\mathbf{x})^2}{\sigma_{i,\text{odo}}^2} \tag{24}$$

and the term related to the prior $\tilde{\mathrm{c}}_{\text{prior}}(\mathbf{x})$

$$\tilde{\mathrm{c}}_{\text{prior}}(\mathbf{x}) = \sum_{i=1}^{K} \frac{\tilde{\mathrm{e}}_{i,s}(\mathbf{x})^2}{\sigma_{i,s}^2} + \sum_{i=1}^{N} \tilde{\mathbf{e}}_{i,\mathbf{p}}(\mathbf{x})^\top \boldsymbol{\Sigma}_{i,\mathbf{p}}^{-1} \tilde{\mathbf{e}}_{i,\mathbf{p}}(\mathbf{x}) \ . \tag{25}$$

To get the LS estimate around the current working point we set the gradient of $\tilde{\mathrm{c}}(\mathbf{x})$ to zero

$$\nabla_{\mathbf{x}} \tilde{\mathrm{c}}(\mathbf{x}) = \nabla_{\mathbf{x}} \tilde{\mathrm{c}}_{\text{lik}}(\mathbf{x}) + \nabla_{\mathbf{x}} \tilde{\mathrm{c}}_{\text{prior}}(\mathbf{x}) = \mathbf{0}_{\dim(\mathbf{x})\times 1} \ . \tag{26}$$

The gradient for the likelihood term is given by

$$\begin{aligned}\nabla_{\mathbf{x}} \tilde{\mathrm{c}}_{\text{lik}}(\mathbf{x}) = &\sum_{i=1}^{|\mathcal{Z}_\tau|} \frac{2}{\sigma_{i,\tau}^2} \mathbf{J}_{i,\tau}^\top \, \mathrm{e}_{i,\tau}(\mathbf{x}_*) + \frac{2}{\sigma_{i,\tau}^2} \mathbf{J}_{i,\tau}^\top \mathbf{J}_{i,\tau} \Delta\mathbf{x} \\ &+ \sum_{i=1}^{|\mathcal{Z}_{\text{mag}}|} \frac{2}{\sigma_{\text{mag}}^2} \mathbf{J}_{i,\text{mag}}^\top \, \mathrm{e}_{i,\text{mag}}(\mathbf{x}_*) + \frac{2}{\sigma_{\text{mag}}^2} \mathbf{J}_{i,\text{mag}}^\top \mathbf{J}_{i,\text{mag}} \Delta\mathbf{x} \\ &+ \sum_{i=1}^{|\mathcal{Z}_{\text{odo}}|} \frac{2}{\sigma_{\text{odo}}^2} \mathbf{J}_{i,\text{odo}}^\top \, \mathrm{e}_{i,\text{odo}}(\mathbf{x}_*) + \frac{2}{\sigma_{\text{odo}}^2} \mathbf{J}_{i,\text{odo}}^\top \mathbf{J}_{i,\text{odo}} \Delta\mathbf{x} \ , \end{aligned} \tag{27}$$

where $\Delta\mathbf{x} = \mathbf{x} - \mathbf{x}_*$ is used for brevity. For the prior term the gradient is

$$\begin{aligned}\nabla_{\mathbf{x}} \tilde{\mathrm{c}}_{\text{prior}}(\mathbf{x}) = &\sum_{i=1}^{K} \frac{2}{\sigma_{i,s}^2} \mathbf{J}_{i,s}^\top \, \mathrm{e}_{i,s}(\mathbf{x}_*) + \frac{2}{\sigma_{i,s}^2} \mathbf{J}_{i,s}^\top \mathbf{J}_{i,s} \Delta\mathbf{x} \\ &+ \sum_{i=1}^{N} 2\mathbf{J}_{i,\mathbf{p}}^\top \boldsymbol{\Sigma}_{i,\mathbf{p}}^{-1} \, \mathbf{e}_{i,\mathbf{p}}(\mathbf{x}_*) + 2\mathbf{J}_{i,\mathbf{p}}^\top \boldsymbol{\Sigma}_{i,\mathbf{p}}^{-1} \mathbf{J}_{i,\mathbf{p}} \Delta\mathbf{x} \ . \end{aligned} \tag{28}$$

Equation (26) can be expressed as a linear system of equations

$$-\mathbf{a} = \mathbf{H} \Delta\mathbf{x} \ , \tag{29}$$

with vector

$$\begin{aligned}\mathbf{a} = &\sum_{i=1}^{|\mathcal{Z}_\tau|} \frac{2}{\sigma_{i,\tau}^2} \mathbf{J}_{i,\tau}^\top \, \mathrm{e}_{i,\tau}(\mathbf{x}_*) + \sum_{i=1}^{|\mathcal{Z}_{\text{mag}}|} \frac{2}{\sigma_{\text{mag}}^2} \mathbf{J}_{i,\text{mag}}^\top \, \mathrm{e}_{i,\text{mag}}(\mathbf{x}_*) \\ &+ \sum_{i=1}^{|\mathcal{Z}_{\text{odo}}|} \frac{2}{\sigma_{\text{odo}}^2} \mathbf{J}_{i,\text{odo}}^\top \, \mathrm{e}_{i,\text{odo}}(\mathbf{x}_*) + \sum_{i=1}^{K} \frac{2}{\sigma_{i,s}^2} \mathbf{J}_{i,s}^\top \, \mathrm{e}_{i,s}(\mathbf{x}_*) \\ &+ \sum_{i=1}^{N} 2\mathbf{J}_{i,\mathbf{p}}^\top \boldsymbol{\Sigma}_{i,\mathbf{p}}^{-1} \, \mathbf{e}_{i,\mathbf{p}}(\mathbf{x}_*) \end{aligned} \tag{30}$$

and matrix

$$\begin{aligned}\mathbf{H} = &\sum_{i=1}^{|\mathcal{Z}_\tau|} \frac{2}{\sigma_{i,\tau}^2} \mathbf{J}_{i,\tau}^\top \mathbf{J}_{i,\tau} + \sum_{i=1}^{|\mathcal{Z}_{\text{mag}}|} \frac{2}{\sigma_{\text{mag}}^2} \mathbf{J}_{i,\text{mag}}^\top \mathbf{J}_{i,\text{mag}} \\ &+ \sum_{i=1}^{|\mathcal{Z}_{\text{odo}}|} \frac{2}{\sigma_{\text{odo}}^2} \mathbf{J}_{i,\text{odo}}^\top \mathbf{J}_{i,\text{odo}} + \sum_{i=1}^{K} \frac{2}{\sigma_{i,s}^2} \mathbf{J}_{i,s}^\top \mathbf{J}_{i,s} \\ &+ \sum_{i=1}^{N} 2\mathbf{J}_{i,\mathbf{p}}^\top \boldsymbol{\Sigma}_{i,\mathbf{p}}^{-1} \mathbf{J}_{i,\mathbf{p}} \ . \end{aligned} \tag{31}$$

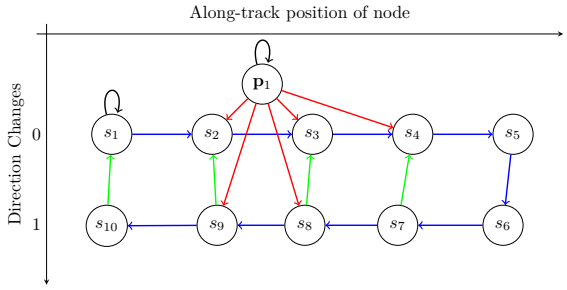

Figure 4. Pose-graph with ten along-track positions and one transmitter. Odometer measurements are shown as blue lines, loop closures as green lines, and prior information is shown as black loops from a node to itself. Since the along-track position is one-dimensional and the nodes will overlap when drawn on a line, we introduced an artificial discrete dimension that represents how often the train has changed its driving direction since the start of the measurements. The 3D transmitter position cannot be properly shown in this coordinate system and is just added for illustration, where the red edges represent TDoA measurements.

With (29)–(31) we can now solve the optimization problem by first solving for $\Delta\mathbf{x}$ and then calculating the new state estimate from it

$$\hat{\mathbf{x}} = \mathbf{x}_* - \mathbf{H}^{-1}\mathbf{a} \ . \tag{32}$$

Since the estimation problem is nonlinear, we have to repeat this process multiple times until $\Delta\mathbf{x}$ becomes sufficiently small and the estimated $\hat{\mathbf{x}}$ has converged.

E. Problem Structure

The pose-graph of the proposed SLAM algorithm contains a node for each along-track train position s and each transmitter position $\mathbf{p}$ in $\mathbf{x}$. The graph is sparse, which here means each node is only connected directly to a few other nodes. There is always an edge between two consecutive s representing an odometer measurement. In addition, there might be an edge between two non-consecutive s when a loop closure was detected from the magnetic field. For the transmitter positions, the situation is a bit different. Each $\mathbf{p}$ is connected to multiple s, where an edge represents a TDoA measurement. A simple example pose-graph for the proposed SLAM algorithm is shown in Fig. 4.

Matrix $\mathbf{H}$ and vector $\mathbf{a}$ in (29) are a mathematical representation of the graph structure and since the pose-graph is sparse also the matrix and the vector are sparse. This becomes also clear when we look at the Jacobians, which contain only a few non-zero elements. The sparseness enables the use of sparse solvers for (29) and thus also large SLAM problems, e.g., long railway tracks can be handled.

III. Evaluation

The evaluation uses real measurements for the odometer and magnetometer data and simulated data for the TDoAs. In the following, we will briefly describe the measurement setup and the simulation parameters.

Figure 5. Track in Berlin between Grunewald and Halensee (red line). The starting position of the different runs is marked by a red dot. The three transmitter positions simulated in the evaluation are marked by a green triangle. Image data: Google Earth.

Table I
SIMULATED SIGNAL PARAMETERS AND TRANSMITTER PLACEMENT ORIENTED ON FRMCS [12]

Parameter Name		Value
Transmit Power	P_{Tx}	40 dBm
Bandwidth	B	10 MHz
Effective bandwidth	β^2	$\frac{B^2}{12}$
Carrier frequency	f_{c}	1905 MHz
Wavelength	λ	$\frac{c}{f_{\text{c}}}$
Antenna Temperature	ϑ	300 K

A. Measurement Setup

The used measurements are identical to the data in [9] and were recorded with the advanced TrainLab of the Deutsche Bahn while driving through Berlin. The sensor hardware consists of a low-cost Kionix KMX62 magnetometer to measure the magnetic vector field with 200 Hz and a DEUTA wheel encoder for the 1 Hz odometer measurements. The ground truth positions are obtained with a Septentrio GNSS receiver.

For the measurements, we use the 2.2 km long track segment shown in Fig. 5. The evaluation is based on four roughly 1.7 km long runs on the shown track, where each run starts at the red dot from which the train drives towards Grunewald, where it stops. From Grunewald, the train then drives towards Halensee and back to the starting point. In the measurements, the train was actually not stopping at Halensee because of operational requirements but instead it was driving past that point and returned only after a few minutes. To limit the data to the shown track, all data beyond Halensee was cut, which results in a discontinuity in the measurements as explained also in [9]. To cope with the discontinuity, a virtual odometer measurement, constructed from the ground truth position obtained with GNSS, is inserted into the sequence of odometer measurements at the time of the discontinuity.

B. Simulation of TDoA Measurements

In contrast to the magnetic field and odometer data, TDoAs were not measured during the runs and thus have to be simulated. In the simulation, a TDoA is obtained by inserting the GNSS ground truth train position and the chosen transmitter positions into (3). On the resulting TDoA, we then add measurement noise depending on the distance of the two train antennas to the transmitter antenna. The variance of the noise is calculated based on the Cramér-Rao lower bound (CRLB) for TDoA [10]

$$\sigma_\tau^2 = \frac{2c^2 k_{\text{b}} \vartheta B}{\lambda^2 \beta^2 P_{\text{Tx}}} \left(\|\mathbf{m}(s_j) - \mathbf{p}_l\|^2 + \|\mathbf{m}(s_j - b) - \mathbf{p}_l\|^2 \right) , \quad (33)$$

where c is the speed of light and k_{b} the Boltzmann constant. The remaining parameters from (33) are defined in Table I. The signal parameters and the positioning of the transmitter are based on what is proposed for FRMCS in [12]. Since in [12] for urban environments only every 2 km or 4 km a transmitter is foreseen, we assume here the worst case of 4 km and simulate only one transmitter next to the track. To investigate how the transmitter position influences the SLAM algorithm, we simulate scenarios with three different transmitter positions as shown in Fig. 5. In accordance with [12], in all scenarios the transmitter has a distance of 15 m to the track and an antenna height of 20 m, the train antenna height is set to 4 m. The simulated TDoAs are rather optimistic since we only consider free space path loss and line of sight conditions. This results in a noise standard deviation of only a few centimeters down to millimeters. Under real propagation conditions, this is most likely not the case. Nevertheless, the simulation gives us an idea if the proposed method has merit and should be further investigated with more realistic channel models or actual measurements.

C. Graph Generation

In order to run the optimization algorithm, the pose-graph has to be constructed. In the evaluation, we add a new pose node whenever the train has traveled at least 25 m since the last node was added. Whenever a node is added, the occurrence of a magnetic loop closure is checked and a corresponding edge is added if one is detected. For the loop closure detection local maps with 100 m length and magnetic signatures of 50 m are used.

Consecutive pose nodes are always connected by an odometer edge representing the measured along-track distance between them. For each pose node, we also add an TDoA edge since we assume full coverage of the transmitter in the simulation scenario. When the first TDoA edge is created, we also add the corresponding transmitter position node to the graph. The initial transmitter position is set to the current train position and a height of 100 m due to the lack of a better initial guess. A prior for the transmitters is not used here and was introduced only for completeness.

D. Initialization and Parameters

In the evaluation, it is assumed that the position of the first along-track node is known. This is included in the optimization by setting a prior of the first node with small variance and a mean at the true position. For a perfectly straight track this prior information is crucial because otherwise the SLAM problem has no unique solution. For a track with curves, this information might not be needed but certainly helps the algorithm to converge to a good solution. Under which conditions

Table II
ALONG-TRACK POSITION ERROR STATISTICS FOR DIFFERENT SLAM VERSIONS AND TRANSMITTER POSITIONS.

	Run 1		Run 1-2		Run 1-3		Run 1-4	
	RMSE/m	max/m	RMSE/m	max/m	RMSE/m	max/m	RMSE/m	max/m
`odometry`	1.85	4.52	3.11	6.20	4.67	10.20	6.52	12.87
`mag`	1.00	3.13	1.04	3.11	1.10	3.06	1.06	3.12
`TDoA(1)`	1.36	3.10	1.41	3.03	1.43	3.41	1.23	2.82
`TDoA(2)`	0.77	2.53	0.73	2.82	0.77	2.82	0.76	2.73
`TDoA(3)`	1.58	3.42	2.10	3.59	2.08	3.42	2.05	3.37
`full(1)`	1.53	3.04	1.59	2.95	1.09	2.38	0.97	2.22
`full(2)`	0.81	2.57	0.72	2.41	0.72	2.32	0.75	2.39
`full(3)`	0.99	3.01	1.14	2.66	1.43	2.81	1.48	2.8

Table III
TRANSMITTER POSITION ERROR STATISTICS FOR DIFFERENT SLAM VERSIONS AND TRANSMITTER POSITIONS.

	Run 1		Run 1-2		Run 1-3		Run 1-4	
	$\epsilon_{\mathbf{p}}$/m	$\mathrm{tr}(\hat{\mathbf{\Sigma}})/\mathrm{m}^2$	$\epsilon_{\mathbf{p}}$/m	$\mathrm{tr}(\hat{\mathbf{\Sigma}})/\mathrm{m}^2$	$\epsilon_{\mathbf{p}}$/m	$\mathrm{tr}(\hat{\mathbf{\Sigma}})/\mathrm{m}^2$	$\epsilon_{\mathbf{p}}$/m	$\mathrm{tr}(\hat{\mathbf{\Sigma}})/\mathrm{m}^2$
`TDoA(1)`	1.35	0.21	1.25	0.17	1.04	0.12	1.12	0.07
`TDoA(2)`	0.86	0.18	0.71	0.13	0.77	0.07	0.73	0.06
`TDoA(3)`	1.21	4.15	1.49	2.44	1.69	1.87	1.61	1.48
`full(1)`	1.45	0.15	1.47	0.11	1.40	0.07	1.52	0.03
`full(2)`	0.90	0.18	0.73	0.13	0.86	0.07	0.86	0.06
`full(3)`	1.62	3.00	1.83	1.73	2.01	1.36	1.96	1.18

prior information is not needed is an interesting aspect that should be explored in future work. For the remaining nodes no prior is used.

For the optimization, the variances of the different measurements have to be set to weight them relative to each other. For the TDoA, the actual value of the standard deviation is changing depending on the distance to the transmitter but since the distance is unknown to the estimator we cannot assume to have this information during the optimization. Therefore, here a conservative value of $\sigma_{i,\tau} = 0.15\,\mathrm{m}$ was chosen. For the magnetic loop closures and the odometer $\sigma_{i,\mathrm{mag}} = 1\,\mathrm{m}$ and $\sigma_{i,\mathrm{odo}} = 0.5\,\mathrm{m}$ is used. As a benchmark, we will also run the SLAM algorithm without TDoAs. For this we keep the parameters $\sigma_{i,\mathrm{mag}} = 0.1\,\mathrm{m}$ and $\sigma_{i,\mathrm{odo}} = 1\,\mathrm{m}$ from [9]. For the baseline between the train antennas a value of 20 m is selected. This allows that both antennas are placed on the same wagon of a modern high speed train. In the evaluation, a Monte Carlo simulation was performed and the SLAM algorithm is evaluated 100 times for each transmitter position to see the impact of different noise realizations.

E. Results

In the following, the term `odometry` is used for the pure odometry solution and `mag` for the SLAM approach with magnetic loop closures from [9]. The terms `TDoA(`l`)` and `full(`l`)` describe the SLAM versions that combine the odometry with TDoAs or with TDoAs and the magnetic loop closures. The index l simply stands for the transmitter position in the simulation.

Table II shows the position root mean square error (RMSE) and the maximum absolute error (max) of the train position

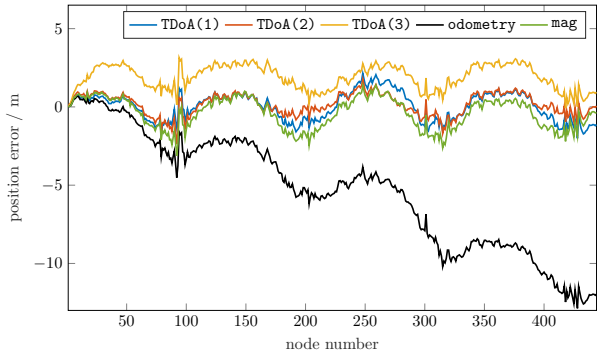

Figure 6. Along-track position error for the SLAM approach that uses only TDoA and odometer measurements. As a benchmark, also the error of the pure odometry and the magnetic field SLAM approach is shown. The shown errors are the difference of the GNSS ground truth and the estimate along-track positions of the nodes.

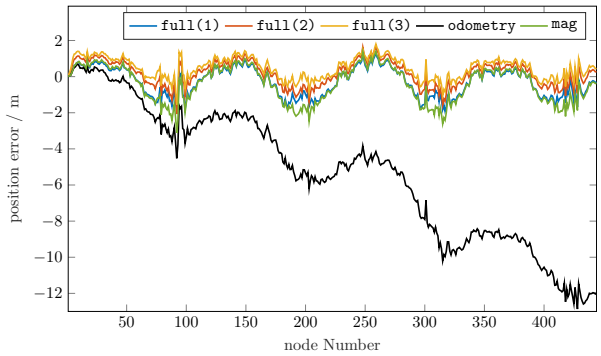

Figure 7. Along-track position error for the SLAM approach that combines the TDoA and odometer measurements with magnetic loop closures.

nodes after one, two, three, or four runs on the track in Berlin. For the algorithms that use TDoA, the shown values are the highest values over all Monte Carlo runs. The results clearly show that using only the TDoA from a single transmitter at an unknown position already can improve and bound the error of the odometry. The achievable error depends on the position of the transmitter. Placing the transmitter at $\mathbf{p}_2$, next to the start position, achieved the best results. One reason for this might be that the transmitter is roughly in the middle of the track and therefore the maximum distance to the train antennas is the lowest. Another reason is the accuracy of the estimated transmitter position discussed in the next paragraph. When in addition to the TDoAs the magnetic field is used, the results are mixed and after the first runs the errors are not always improved compared to the TDoA only case. After processing all four runs, this is no longer the case and all errors are reduced. For all transmitter positions the maximum error could be reduced by combining TDoA and magnetic loop closures compared to only using the magnetic field. Interestingly, for the RMSE this is not always the case. We can only speculate about the reason for this but one reason could be rooted in the AWGN assumption for all measurements, which is not fulfilled for the odometry and magnetic loop closures. To see this and to get a better impression of the train position error,

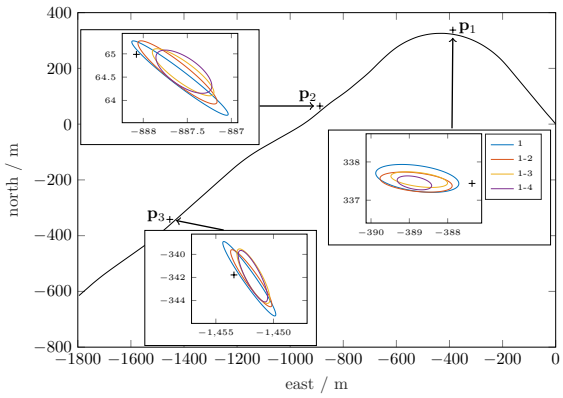

Figure 8. Distribution of transmitter position estimates for the full SLAM algorithm. The ellipses are centered at the sample mean and are derived from the sample covariance matrices and are scaled to represent "three sigma" areas. The different colors show the result after processing 1, 2, 3, or 4 runs. The true transmitter positions are shown as black "+".

Fig. 6 and Fig. 7 show the position error for each node and the different SLAM versions and transmitter positions. The shown values are always the ones with the highest RMSE and after processing four runs. The figures show that the odometry error has a linear drift with a superimposed oscillation. All SLAM versions are able to remove the linear drift but cannot fully remove the oscillation.

For the estimated transmitter positions, the error statistics are calculated over the 100 Monte Carlo runs and are shown in Table III. Concretely, the Euclidean norm $\epsilon_{\mathbf{p}}$ of the position estimation bias and the trace $\mathrm{tr}(\hat{\mathbf{\Sigma}})$ of the sample covariance is given for the different SLAM versions. The sample covariance matrices are also shown in Fig. 8. Similar to the train position, placing the transmitter at $\mathbf{p}_2$ gives also the highest accuracy for the transmitter position. This is plausible since for transmitter and train localization the important TDoA measurements are the ones taken in proximity to the transmitter where the TDoA has a strong dependency on the transmitter and train position. Now with that in mind, the best performance of the SLAM algorithm for transmitter position $\mathbf{p}_2$ can be explained. For $\mathbf{p}_2$, the train starting position is directly next to the transmitter and therefore the SLAM algorithm immediately receives TDoA measurements with a good geometry, while at the same time the train position is still accurately known since there was not much time to accumulate position errors and uncertainties.

From Table III it becomes also clear that including magnetic loop closures into the estimation increases the bias of the estimated transmitter positions, again this could be caused by the false AWGN assumptions for the measurements but also by the nonlinearity of the problem which could lead to biased estimates. Besides increasing the bias of the estimation, the magnetic loop closures reduced the overall variance in the estimates, which is reflected in a reduction of the sample covariance compared to the TDoA only case. From Fig. 8 one can also see that by processing more runs the estimates converge towards a steady value.

IV. Conclusion

In this paper, we proposed a novel SLAM algorithm that combines odometer measurements with a magnetic field-based loop closure detection and TDoA measurements to unknown track-side transmitters. The proposed algorithm is based on pose-graph optimization and estimates the along-track train position and the unknown transmitter positions.

The proposed algorithm was evaluated with a data set recorded on a track in Berlin. The data set only contains the measurements of a low-cost magnetometer and a wheel encoder. In order to evaluate the proposed algorithm, the TDoA measurements were simulated using the parameters of FRMCS assuming line of sight and free space path loss. The results of the evaluation showed that the proposed algorithm is capable of estimating the along-track and the transmitter positions with a runtime that was at least 10 times shorter than the data set duration. Furthermore, the results indicate that incorporating TDoA measurements to a single transmitter into the SLAM algorithm can improve the overall position accuracy and bound the position error when magnetic loop closures are not available.

References

[1] B. Siebler, O. Heirich, S. Sand, and U. D. Hanebeck, "Joint Train Localization and Track Identification based on Earth Magnetic Field Distortions," in *2020 IEEE/ION Position, Location and Navigation Symposium (PLANS)*, Apr. 2020, pp. 941–948.

[2] A. Canciani and J. Raquet, "Airborne Magnetic Anomaly Navigation," *IEEE Transactions on Aerospace and Electronic Systems*, vol. 53, no. 1, pp. 67–80, 2017.

[3] J. A. Shockley and J. F. Raquet, "Navigation of Ground Vehicles Using Magnetic Field Variations," *NAVIGATION*, vol. 61, no. 4, pp. 237–252, 2014.

[4] A. Solin, S. Särkkä, J. Kannala, and E. Rahtu, "Terrain navigation in the magnetic landscape: Particle filtering for indoor positioning," in *2016 European Navigation Conference (ENC)*, 2016, pp. 1–9.

[5] M. Frassl, M. Angermann, M. Lichtenstern, P. Robertson, B. J. Julian, and M. Doniec, "Magnetic maps of indoor environments for precise localization of legged and non-legged locomotion," in *2013 IEEE/RSJ International Conference on Intelligent Robots and Systems*, 2013, pp. 913–920.

[6] B. Siebler, T. Gerstewitz, S. Sand, and U. D. Hanebeck, "Magnetic Field-based Indoor Localization of a Tracked Robot with Simultaneous Calibration," in *2023 13th International Conference on Indoor Positioning and Indoor Navigation (IPIN)*, 2023, pp. 1–6.

[7] M. Kok and A. Solin, "Scalable Magnetic Field SLAM in 3D Using Gaussian Process Maps," in *2018 21st International Conference on Information Fusion (FUSION)*, 2018, pp. 1353–1360.

[8] T. N. Lee and A. J. Canciani, "MagSLAM: Aerial simultaneous localization and mapping using Earth's magnetic anomaly field," *NAVIGATION*, vol. 67, no. 1, pp. 95–107, 2020.

[9] B. Siebler, A. Lehner, S. Sand, and U. D. Hanebeck, "Magnetic Field Mapping of Railway Lines with Graph SLAM," in *2024 27th International Conference on Information Fusion (FUSION)*, 2024, pp. 1–8.

[10] B. Siebler, M. Schmidhammer, and S. Sand, "Hyperbolic Vehicle Localization Using a Single Signal of Opportunity and Trajectory Constraints," in *2019 22th International Conference on Information Fusion (FUSION)*, 2019, pp. 1–7.

[11] G. Grisetti, R. Kümmerle, C. Stachniss, and W. Burgard, "A Tutorial on Graph-Based SLAM," *IEEE Intelligent Transportation Systems Magazine*, vol. 2, no. 4, pp. 31–43, 2010.

[12] "ETSI TR 103 554-2 V1.1.1: Rail Telecommunications (RT); Next Generation Communication System; Radio performance simulations and evaluations in rail environment; Part 2: New Radio (NR)," ETSI, Tech. Rep., 2021.